Supplementary Information

Strong magnetic field-dual-assisted fabrication of heterogeneous sulfides hollow nanochains electrodes for high-rate supercapacitors

Xing Yu,[a] Jiali Yu,[a] Yves Fautrelle,[b] Annie Gagnoud,[b] Zhongming Ren,[a] Xionggang Lu,[a] and Xi Li*[ab]

[a]*State Key Laboratory of Advanced Special Steels, School of Materials Science and Engineering, Shanghai University, Shanghai 200072, P. R. China. E-mail: lx_net@sina.com*
[b]*SIMAP-EPM-Madylam/G-INP/CNRS, ENSHMG, BP 38402 St Martin d'Heres Cedex, France*

Experimental

Synthesis of Co-based glycolate precursors: Typically, 0.4 g polyvinyl pyrrolidone (PVP, Mw ~58,000) was dissolved in ethylene glycol (EG). 0.5 g $Co(CH_3COO)_2 \cdot 4H_2O$ and 55 mg $Zn(CH_3COO)_2 \cdot 2H_2O$ were then added into the above transparent solution. Afterward, the obtained mixed solution was transferred into a round bottom flask and refluxed at 170 °C for 2 h in an oil bath. After the solution was cooled down naturally, a purple precipitate, namely CZ_{55}-glycolate, was collected by centrifugation. For comparison, different Co-based glycolate precursors were prepared through the same process and marked as C-glycolate, CZ_{35}-glycolate and CM_{51}-glycolate, respectively, by altering the amount of $Zn(CH_3COO)_2 \cdot 2H_2O$ such as 0 and 35 mg, and substituting $Zn(CH_3COO)_2 \cdot 2H_2O$ with other acetates such as $Mn(CH_3COO)_2 \cdot 4H_2O$.

Synthesis of the hollow $CZ_{55}S^{6T}$ nanochains: First, 30 mg CZ_{55}-glycolate was dispersed into pure ethanol by ultrasonic. After that, 60 mg thioacetamide (TAA) was added to the suspension under vigorous stirring. Then, the mixture was put into a Teflon-lined autoclave, which was subsequently placed in a superconducting magnet (OXFORD) with a field strength of 6T, and maintained at 160 °C for 2 h. After centrifugation and wash with ethanol for three times, the black powder of $CZ_{55}S^{6T}$ HNCs was obtained by drying in vacuum. For comparison, different field strengths such as 0T, 1T, 2T and 3T, and different precursors like C-glycolate, CZ_{35}-glycolate and CM_{51}-glycolate were applied alone, and the corresponding samples were denoted as $CZ_{55}S^{0T}$, $CZ_{55}S^{1T}$, $CZ_{55}S^{2T}$, $CZ_{55}S^{3T}$ and CS^{6T}, $CZ_{35}S^{6T}$, $CM_{51}S^{6T}$.

Materials characterization: The samples were characterized using X-ray diffraction (XRD, Rigaku D/max, Cu Kα radiation, λ = 0.154178 nm), field-emission scanning electron microscopy (FESEM, JSM-6700F, 10 kV), transmission electron microscopy (TEM, JEOL JEM-200CX, 160 kV), high-resolution TEM (HRTEM, JEOL JEM-2100F, 200 kV) equipped with Energy-dispersive X-ray spectroscopy (EDX). The Brunauer–Emmett–Teller (BET) surface area was measured by N_2 adsorption/desorption (Autosorb IQ2 analyzer). The surface elemental composition was determined by X-ray photoelectron spectroscopy (XPS, ESCAlab 250 xi). Magnetic measurements were performed on a commercial Superconducting Quantum Interference Device (SQUID, Quantum Design) magnetometer.

Electrochemical Measurements: Electrochemical measurements were performed on a CHI 760E electrochemical workstation (CH instrument Inc., China) and a LAND battery program-control test system (LAND, Wuhan). The electrochemical performances were first evaluated in 6 M KOH electrolyte by a three-electrode system with a counter electrode (Pt foil) and a reference electrode (saturated calomel electrode, SCE). The working electrode was composed of 70 wt% active materials, 20 wt% multilayer graphene flakes (GF) with average thickness of 2.4 nm (Ningbo Morsh Technology Co., Ltd) and 10 wt% polymer binder (polyvinylidene fluoride, PVDF). For the preparation of oriented $CZ_{55}S^{6T}$/G electrode, the drop-cast and evaporation of electrode suspension under 12T SMF was applied. To prepare the suspension, PVDF was first dissolved into N-methyl-2-pyrrolidone (NMP), the $CZ_{55}S^{6T}$ HNCs were dispersed in NMP by light ultrasonic, and the multilayer GF synthesized via

intercalation and exfoliation of graphite were also dispersed in NMP homogeneously with the help of strong ultrasonic. The former two solutions were first mixed together under vigorous stirring. Afterwards, the third suspension was added to the mixed solution to assist aligning the nanochains and increase both the conductivity and density of the electrode. The as-derived suspension was then cast into a cylindrical plastic mould on a nickel foil under 12T SMF. The NMP solvent was allowed to evaporate at 25 °C. For comparison, the $CZ_{55}S^{6T}$ and $CZ_{55}S^{0T}$ electrodes were fabricated in the same process without magnetic field. The mass loading of each electrode is around 8 mg cm^{-2}. Cyclic voltammetry (CV), galvanostatic charge-discharge (GCD) and cycling GCD measurements were conducted at relatively high rates except the lower ones.

An asymmetric supercapacitor (ASC) device was assembled using the oriented $CZ_{55}S^{6T}$/G electrode as the positive electrode, the activated carbon (AC) as the negative electrode, and a glass fiber filter paper as the separator. A 6 M KOH solution were employed as the electrolyte. The mass ratio of positive electrode to negative electrode was determined based on the well-known charge balance equation (q+ = q-). The mass loading of the AC and $CZ_{55}S^{6T}$/G in the negative and positive electrodes were around 5 and 8 mg cm^{-2}, respectively.

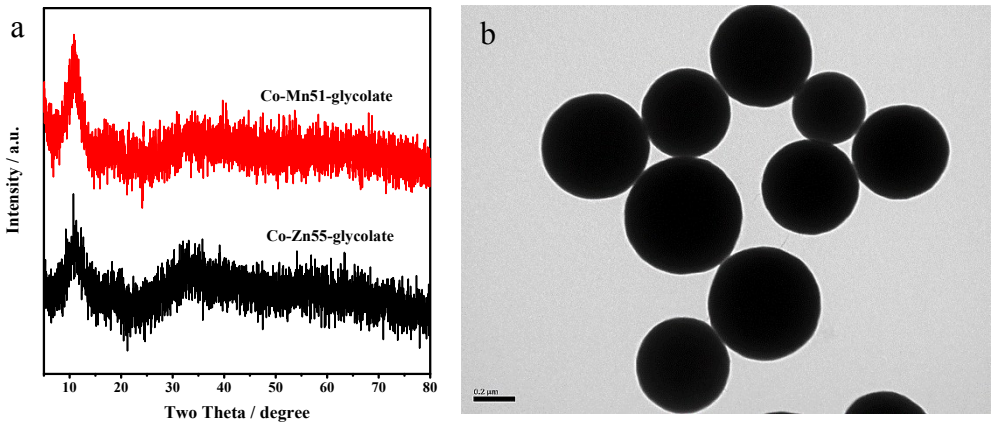

Fig. S1 (a) XRD patterns of the CZ_{55}-glycolate and CM_{51}-glycolate precursors. (b) TEM image of the solid CZ_{55}-glycolate spheres.

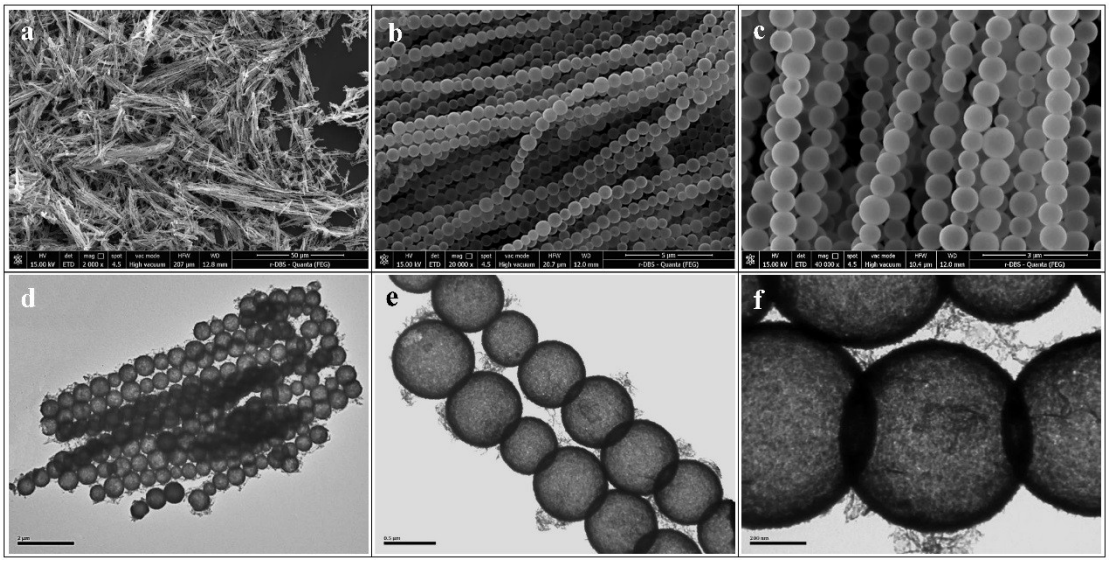

Fig. S2 (a–c) FESEM images and (d–f) TEM images of the $CZ_{55}S^{6T}$ HNCs with different magnifications.

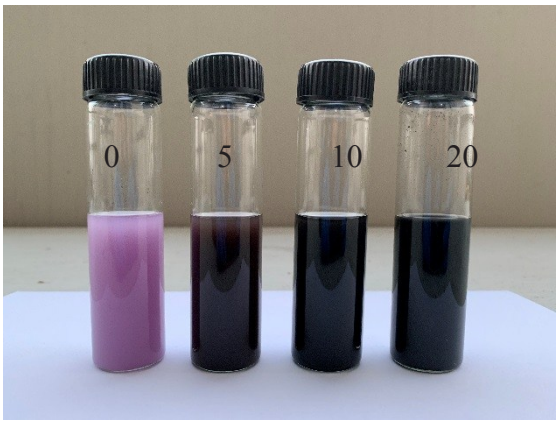

Fig. S3 Digital photo of the intermediates captured after sulfidation reaction for different periods (min) under a 6T SMF, showing the colour change of the intermediates.

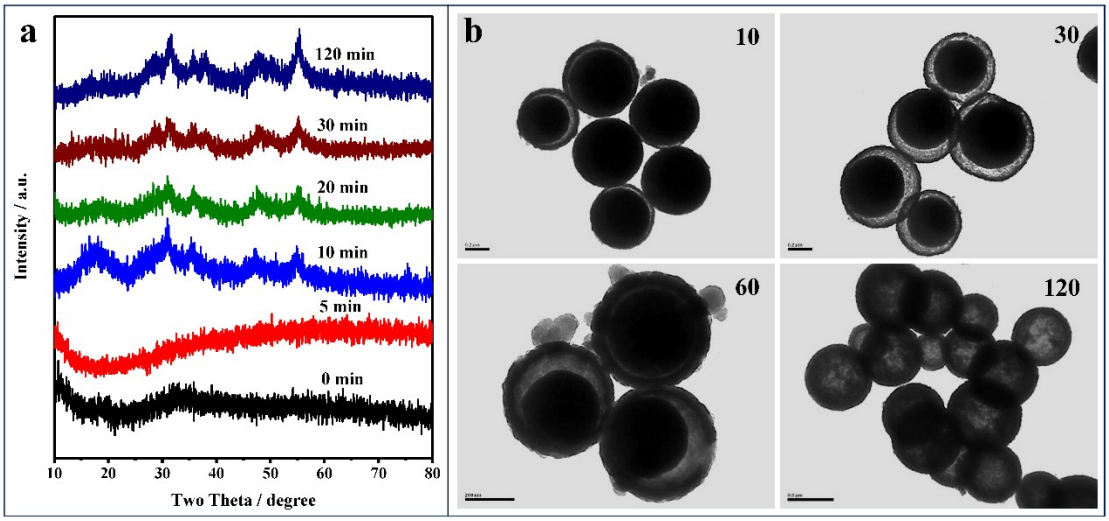

Fig. S4 (a) XRD patterns of the products after sulfidation of CZ_{55}-glycolate for different durations (min) under a 6T SMF. (b) TEM images of the intermediates captured after sulfidation reaction for different durations (min) without magnetic field.

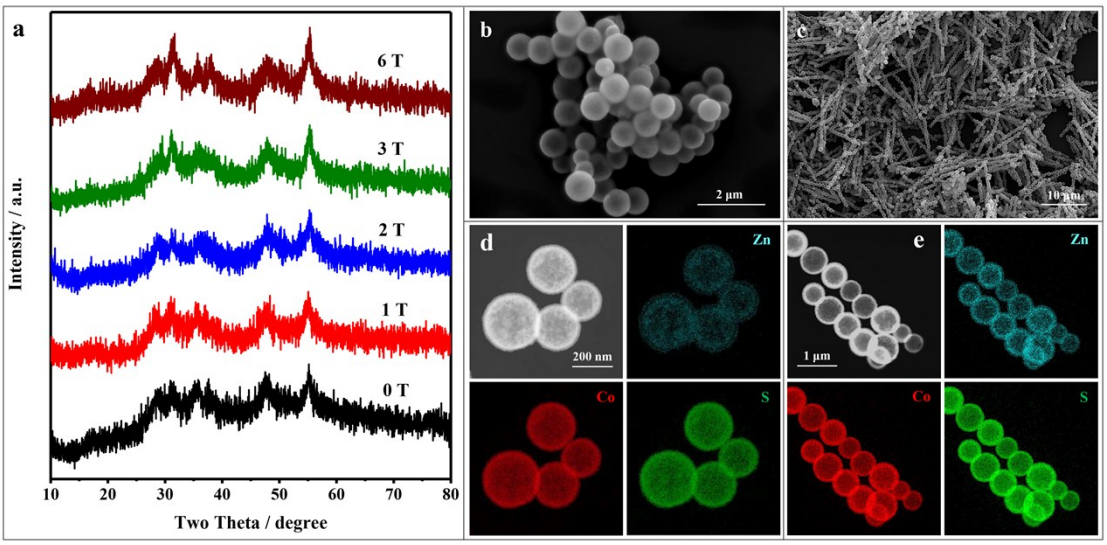

Fig. S5 (a) XRD patterns of products obtained after sulfidation of CZ_{55}-glycolate for 2 h under different magnetic fields. (b) A panoramic FESEM image of $CZ_{55}S^{0T}$ obtained without magnetic field. (c) HAADF-STEM elemental mapping of the $CZ_{55}S^{0T}$ hollow spheres. (d) A panoramic FESEM image of $CZ_{55}S^{3T}$ obtained under a 3T magnetic field. (e) HAADF-STEM elemental mapping of the $CZ_{55}S^{3T}$ HNCs.

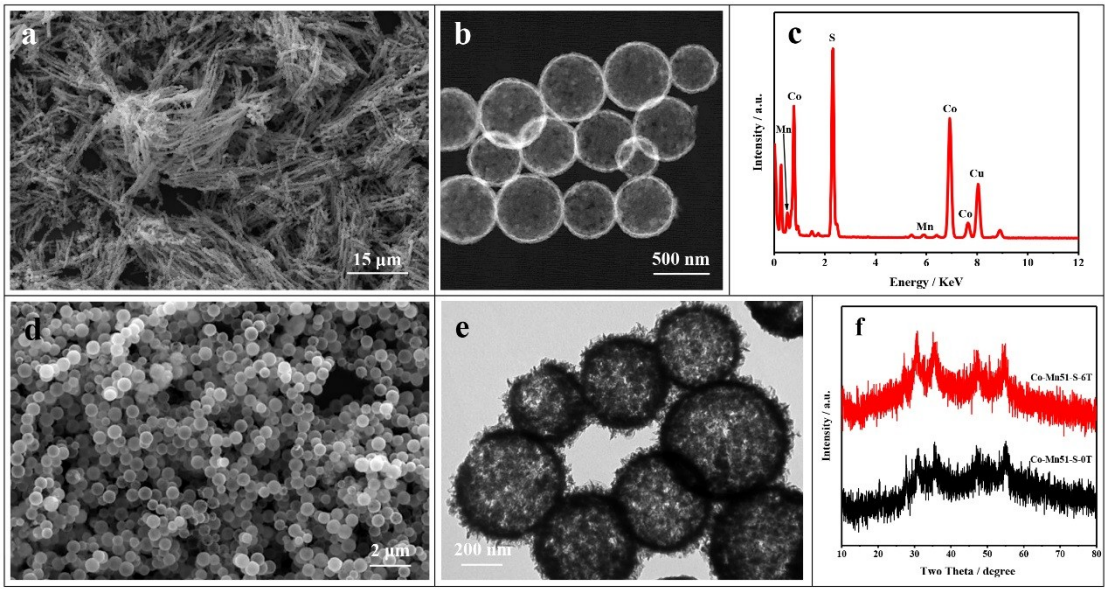

Fig. S6 (a) FESEM, (b) HAADF-STEM images and (c) EDS spectrum of the $CM_{51}S^{6T}$ HNCs obtained after sulfidation of the CM_{51}-glycolate solid spheres for 2 h under a 6T SMF. (d) FESEM, (e) TEM images of the $CM_{51}S^{0T}$ obtained after sulfidation of the CM_{51}-glycolate solid spheres for 2 h without magnetic field. (f) XRD patterns of the as-prepared $CM_{51}S^{0T}$ and $CM_{51}S^{6T}$.

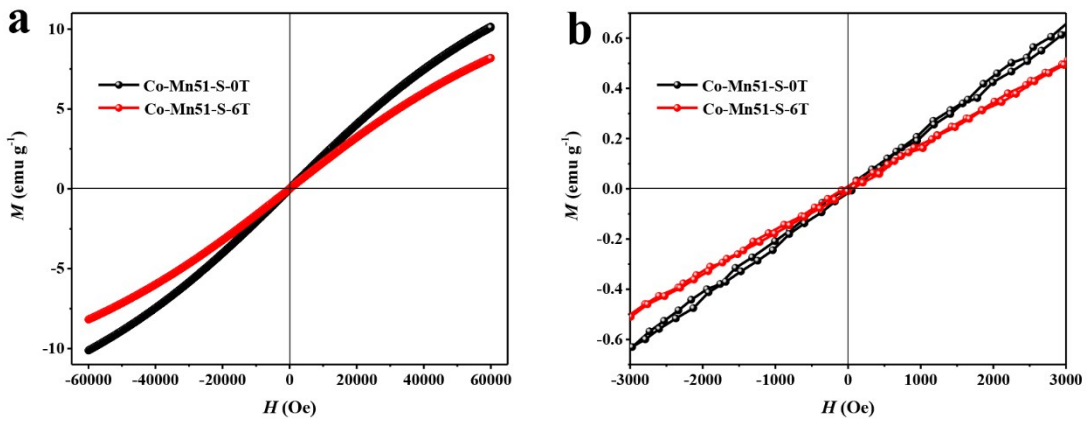

Fig. S7 (a) *M–H* curves and (b) the corresponding enlarged parts of $CM_{51}S^{0T}$ and $CM_{51}S^{6T}$ at 6 K.

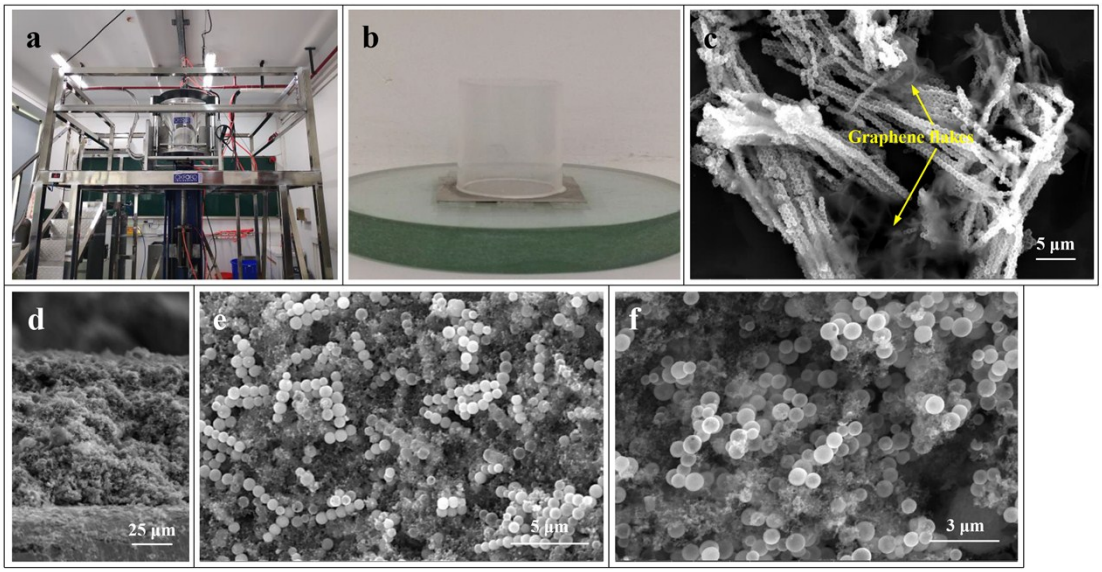

Fig. S8 Photo images of (a) magnetic field apparatus and (b) suspension casting mould. (c) SEM image of $CZ_{55}S^{6T}$/G electrode materials after ultrasonic. Cross-sectional SEM image of (d) aligned $CZ_{55}S^{6T}$/G electrode with low magnification, (e) $CZ_{55}S^{6T}$ electrode and (f) $CZ_{55}S^{0T}$ electrode.

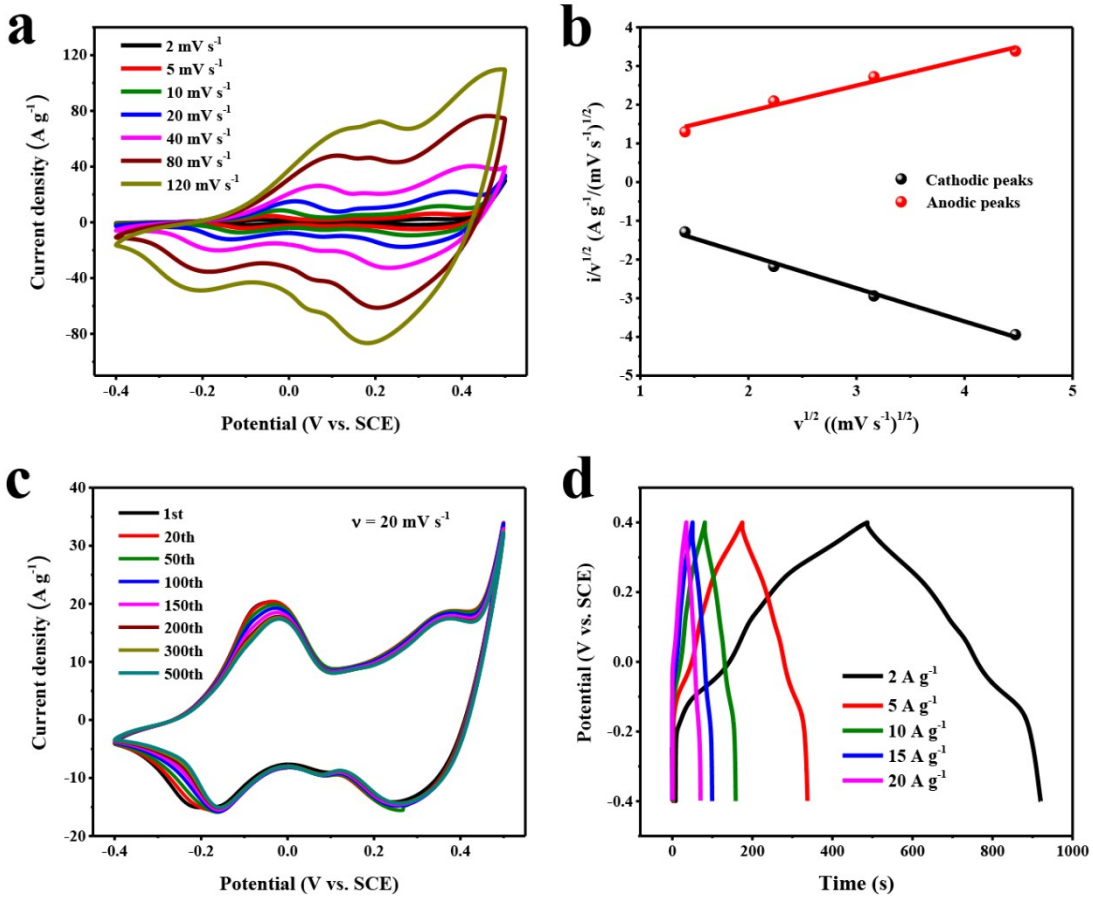

Fig. S9 Electrochemical evaluation of the aligned $CZ_{55}S^{6T}$/G electrode. (a) CV curves at different scan rates. (b) Dependence of the peak current density on square root of scan rate. (c) CV curves (20 mV s^{-1}) with different cycles as indicated. (d) GCD curves at various current densities.

Table S1. The equations based on CV curves of the aligned $CZ_{55}S^{6T}$/G electrode for both anodic and cathodic peaks.

Peak	$i/v^{1/2} = k_1v^{1/2} + k_2$ ($i = k_1v + k_2v^{1/2}$)
Anodic	$i/v^{1/2} = 0.67504v^{1/2} + 0.48281$
Cathodic	$i/v^{1/2} = -0.85673v^{1/2} - 0.1712$

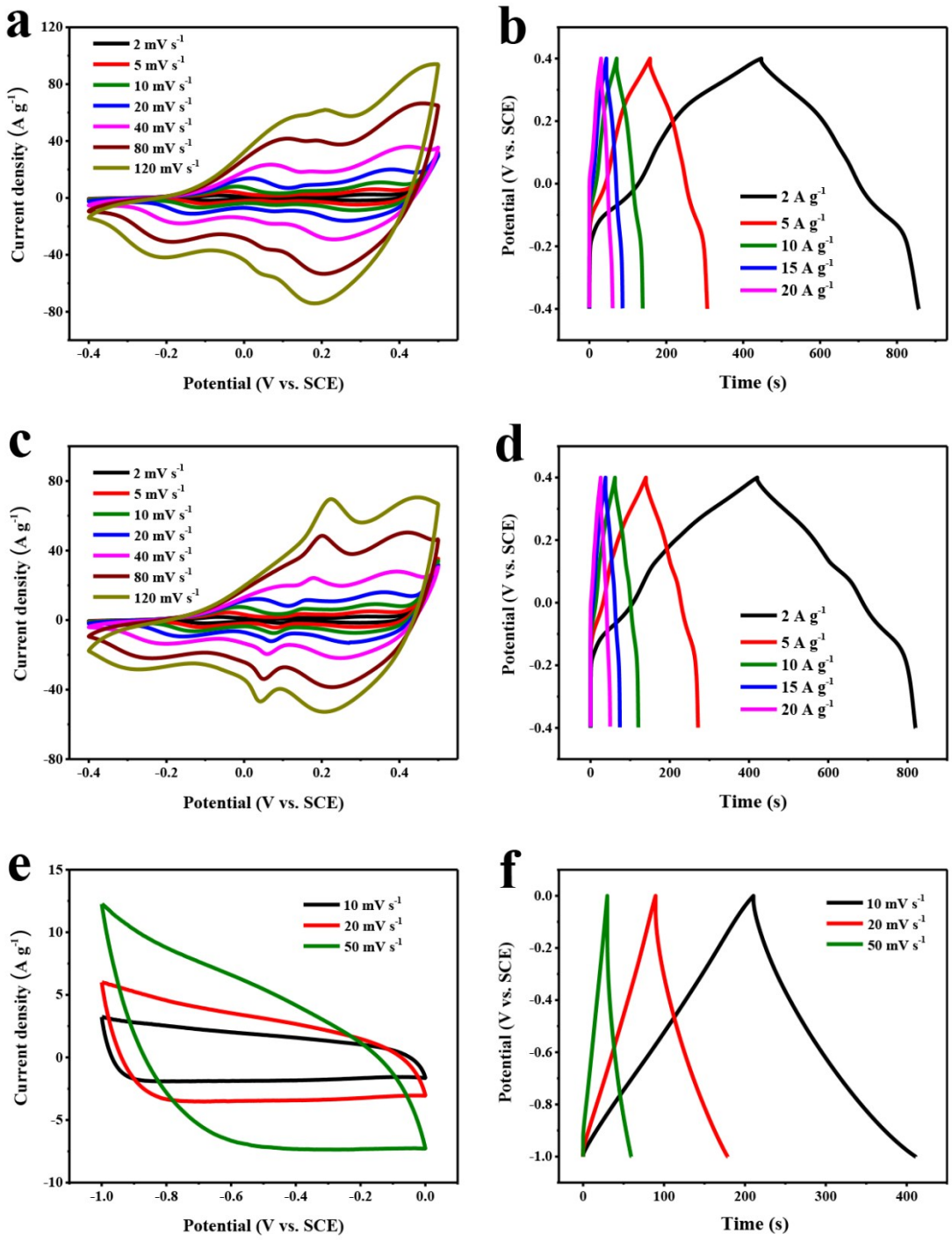

Fig. S10 (a, c, e) CV curves at different scan rates and (b, d, f) GCD curves at various current densities of the (a, b) $CZ_{55}S^{6T}$, (c, d) $CZ_{55}S^{0T}$ and (e, f) activated carbon (AC) electrodes.

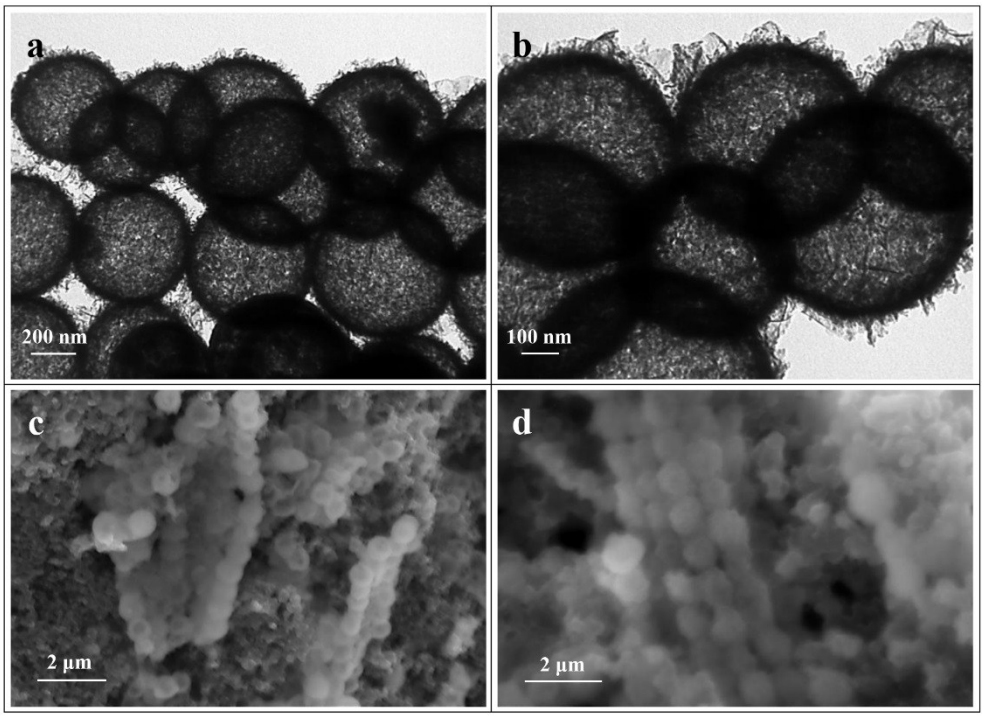

Fig. S11 (a, b) TEM images of the $CZ_{55}S^{6T}$ HNCs after repeated charge/discharge tests. (c, d) Cross-sectional SEM images of the $CZ_{55}S^{6T}$/G electrodes after repeated charge/discharge tests.

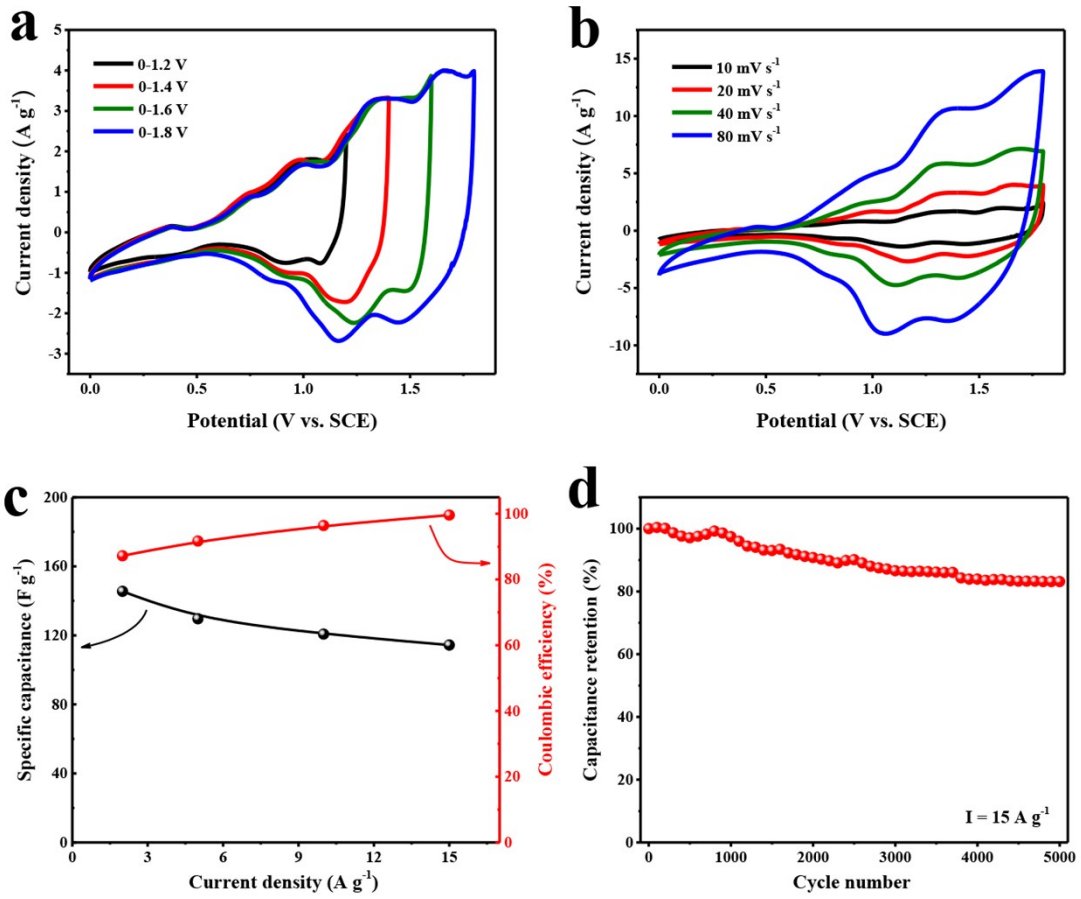

Fig. S12 Electrochemical evaluation of the $CZ_{55}S^{6T}$/G//AC ASC. (a) CV curves under various potential windows at 20 mV s^{-1}. (b) CV curves at different scan rates. (c) Specific capacitance and coulombic efficiency as a function of current density. (d) Cycling performance at a constant current density of 15 A g^{-1}.